Biotribological behavior of Ag-ZrC_xN_{1-x} coatings against UHMWPE for joint prostheses devices

S. Calderon V.[1,2], J.C. Sánchez-López[3], A. Cavaleiro[2], S.Carvalho[1,2]

[1]GRF-CFUM - Physics *Department, University of Minho, 4800-058 Guimarães, Portugal.*

[2]*SEG-CEMUC Mechanical Engineering Department, University of Coimbra, 3030-788 Coimbra, Portugal.*

[3]*Instituto de Ciencia de Materiales de Sevilla (CSIC-US), Avda. Américo Vespucio 49, 41092 Sevilla, Spain.*

Corresponding author*:*

Sebastian Calderon Velasco

Universidade do Minho, Dept. Física, Campus de Azurém, 4800-058 Guimarães, Portugal

Tel: +351- 253510175 ext. 517465

Fax: +351-253510461

Email: ***secave44@gmail.com***

Abstract

This study aims to evaluate the structural, mechanical and tribological properties of zirconium carbonitrides (ZrC_xN_{1-x}) coatings with embedded silver nanoparticles, produced with the intention of achieving a material with enhanced multi-functional properties, including mechanical strength, corrosion resistance, tribological performance and antibacterial behavior suitable for their use in joint prostheses. The coatings were deposited by direct current (DC) reactive magnetron sputtering onto 316L stainless steel, changing the silver content from 0 to 20 at.% by modifying the current density applied to the targets. Different nitrogen and acetylene gas fluxes were used as reactive gases. The coatings revealed different mixtures of crystalline

ZrC_xN_{1-x}, silver nanoparticles and amorphous carbon phases. The hardness of the films was found to be mainly controlled by the ratio between the hard (ZrC_xN_{1-x}) and soft (Ag and amorphous carbon) phases in the films, fluctuating between 7.4 and 20.4 GPa. The coefficient of friction, measured against ultra-high molecular weight polyethylene (UHMWPE) in Hank's balanced salt solution with 10 g L^{-1} albumin, is governed by the surface roughness and hardness. The changes in the UHMWPE wear rate were in the same one order of magnitude (between 1.4 and 2.0 x10^{-6} mm^3 N^{-1} m^{-1}), justified by the effect of the protective layer of albumin formed during the tests. The small differences were due to the hydrophobic/hydrophilic character of the surface, as well as to the silver content.

Keywords: ZrCN, UHMWPE, sputtering, tribology, hardness, amorphous carbon.

1. Introduction

The modification and functionalization of material surfaces have been appealing topics of investigation in the material science and engineering fields, since the surface is the main material portion to interact with the environment. In particular, medical devices, such as surgical tools and prosthesis devices, are particularly interesting in this field due to the need of surface multi-functionality in order to withstand mechanical loading and maintain the biocompatible character, including chemical stability and low tendency to microbial colonization. As a result, multifunctional coatings are being developed in order to improve the current materials used in the medical devices field. The chemical inertness of the materials has been usually achieved by coating the devices with very low reactive ceramic material such as diamond-like-carbon materials [1], nitrides [2] or oxides [3], while the antimicrobial capabilities have been achieved by introducing antimicrobial agents, such as silver [4-9]. The tribological properties, on the other

hand, are strongly dependent on the combination of the materials and lubricant used in the system. For knee and hip joint prosthesis, for instance, 316L stainless steel, Co-Cr-Mo alloys and titanium alloys are usually coupled with ultra-high molecular weight polyethylene (UHMWPE) because of its excellent properties of bio-compatibility, chemical stability, effective impact load damping, low friction coefficient and superior fracture toughness [10, 11]. However, it has been evidenced that the wear of UHMWPE may be the limiting factor that compromises the long-term performance of joint prosthesis [12] by generating polymer debris particles, being highly susceptible to osteolysis, a leading cause of failure for such devices [13]. Thus, specific attention has been placed on the causes of UHMWPE wear.

Several authors have reported that the applied load [10, 14, 15] and the counterpart material properties, like hardness [13], roughness [11-13, 16] and ability to resist particle formation, are the main factors affecting UHMWPE wear. The environment in which the materials interact has also been identified to play a crucial role in the final tribological behavior. Studies about the influence of the different components of the simulated body fluid have demonstrated that the adsorption of proteins strongly affects the wear and coefficient of friction (COF) of the system, depending on the ability of the surface to adsorb such molecules [17]. Albumin absorption reduces the wear rate of the material due to the ability of the adsorbed layer to protect the surface, reducing the material transfer and direct contact between the surfaces up to some extent [18-21]. However, contradictory results have been reported regarding the benefits of the albumin to the friction properties; some reports attribute an increase of COF due to the mutual interactions between the molecules of albumin [22] while others [18-20] state that the protective character of albumin reduces the friction. Thus, surface properties such hydrophobicity and

roughness, known to affect directly the protein adsorption [19, 23], should not be overlooked in regard to their influence on the tribological behavior.

As a result, a material capable of showing a broad scope of all the mentioned properties may be of great importance for evolving the medical devices currently in use. Transition metal carbonitrides (*Me*CN) materials may be good candidates for that purpose. Among the large *Me*CN family of materials, ZrC_xN_{1-x} has been proven to have tunable properties depending on the non-metallic elements contents, altering the hardness, friction coefficient, and biocompatibility in a wide range [24-31]. However, in order to provide the system with antimicrobial capabilities it is necessary to add an antimicrobial agent, such as silver, widely used and proven to be efficient. Nonetheless, adding a fourth element to the ternary system ZrC_xN_{1-x} may alter the properties, highlighting the importance of determining the proper amount of the constituents (Zr, C, N and Ag) to guarantee an appropriate tribological performance.

Consequently, the aim of this work is to evaluate the influence of the chemical, structural and morphological properties of Ag-ZrC_xN_{1-x} films on the tribological performance against UHMWPE as counterpart in biological medium. This analysis will help to assess the viability of this system to be used in the field of prosthetic devices. The Ag-ZrC_xN_{1-x} films would work as a multifunctional coating in which the silver serves as an antibacterial material, the coating itself as a barrier for the delivery of ions from the substrate (SS316L), and the mixture of hard and soft phases as a composite material that enhance the mechanical and tribological performance without compromising the UHMWPE.

2. Materials and Methods

2.1 Coating production

Direct current (DC) unbalanced reactive magnetron sputtering was used to deposit Ag-ZrC_xN_{1-x} films. The sputtering reactor consists of two magnetrons equipped with pure Zr (99.2 at. %, 100 × 200 × 6 mm^3) and Ag (99.9 at. % 100 ×200 ×6 mm^3) targets located in opposite positions in a closed magnetic field configuration and a rotational substrate holder located at 70 mm from the targets. A Joule effect resistor positioned at 80 mm from the substrates is used to regulate the temperature of the chamber and a gas inlet is located in one side of the reactor, homogenizing the gases throughout a gas pipe around the chamber.

Table 1 shows the deposition parameters and variables monitored during the process. The chamber base pressure was set between 2.4 $x10^{-4}$ and 4.2 $x10^{-4}$ Pa and the depositions were carried out using two different acetylene (1.2 and 2.4 sccm) and nitrogen fluxes (3 and 9 sccm), attaining working pressures between 0.60 and 0.69 Pa. The zirconium target current density was maintained at 10 mA cm^{-2}, while the silver target current density was varied between 0.25 and 0.75 mA cm^{-2} to tune the silver content in the films. The bias voltage (-50 V), substrate rotation speed (8 rpm) and chamber temperature (100 ^oC) were monitored and kept constant for all the depositions.

Mirror polished samples of 316L stainless steel and silicon (100) were used as substrates. The 316L substrates were polished using emery paper (from 240 to 2400 grit) and then mirror polished with a diamond solution to obtain surface roughness lower than 8 nm. The samples were cleaned by means of an ultrasonic bath in distilled water, ethanol and acetone during 10 min, to enhance the film adhesion. An in situ etching process, immediately before the coatings production, was carried out using argon atmosphere and a pulsed power supply. Thereafter, a 200 nm Zr interlayer was deposited before the multifunctional Ag-ZrC_xN_{1-x} layer to further enhance the adhesion between the film and the substrate.

2.2 Structural and chemical characterization

The structure was studied by X-ray diffraction in a PANalytical XPert PRO micro-diffractometer with Cu Kα (1.540598 Å) radiation in a grazing angle mode at 3° incidence angle. Thicknesses were evaluated by the Calotest method utilizing a rotation sphere 20 mm in diameter at 1000 rpm for 90 s in order to obtain the desired wear.

The surface morphology and cross section morphology of the films were assessed using a NanoSEM - FEI Nova 200 scanning electron microscope, with a secondary electron detector. Energy dispersive X-ray spectroscopy was utilized to determine changes on the composition after the tribological test. The acceleration voltage was kept at 10 keV for both images and chemical composition analysis.

The surface roughness of the bare and coated steel was measured with a contact stylus profilometer, using 10 mm of distance at 0.1 mm/s of scanning speed. Ra and Rq values were obtained as an average of 5 measurements in different zones of the films.

Raman spectra measurements (200–2000 cm^{-1}) were carried out to the samples using a LabRAM Horiba Jobin Yvon spectrometer equipped with a CCD (charge-coupled device) detector and a He–Ne laser (532 nm) at 5 mW before and after the tribological test, in order to determine alterations on the chemical structure of the films.

The coating chemical composition was analyzed by a Cameca SX 50 electron probe micro-analyzer (EPMA), using statistical analysis of 5 randomly selected spots in each sample. The phase composition was then calculated considering that the ZrC_xN_{1-x} phase possesses all the Zr atoms available in the films (disregarding oxygen contamination) and, therefore, carbon-containing phases are formed by the carbon and nitrogen in excess ([C]+[N]-[Zr]) measured by

EPMA. The number of atoms in the silver state corresponds exactly to the measured atomic percentage. Nonetheless, it must be stressed that the presence of residual oxygen in the system indicates oxides formation, most probably of Zr, as previously shown [32], and therefore, the phase estimation should only be taken as an approximation.

2.3 Mechanical characterization

The hardness and Young modulus were evaluated by a MicroMaterials Nanotest system equipped with a Berkovich indenter at a maximum load of 5 mN. The indenter was maintained 5 s at maximum load and 30 s at lower load for the thermal drift. The loading and unloading rates were maintained equal at 0.167 mN s^{-1}. The values reported are an average of 16 points measured.

2.4 Tribological characterization

The tribological properties were evaluated by reciprocating friction tests using 10 mm ultrahigh molecular weight polyethylene (UHMWPE CHIRULEN 1020) balls in Hank´s balanced salt solution (HBSS) with 10 g L^{-1} of albumin from bovine serum (BSA) at 37 ^{o}C in a CSM ball-on-disk tribometer. The test parameters were set to 10 N of applied load; 20 mm/s of linear speed; 10 mm track length; 80000 cycles of duration at 1 Hz of acquisition rate. Under these conditions, the corresponding initial Hertzian contact pressure was calculated in 40 MPa.

The specific UHMWPE wear rate was calculated as the volume of the spherical cap corresponding to the worn area measured on the UHMWPE, divided by the applied load and the total sliding distance. This wear rate value is believed to be overestimated since the surface of

the UHMWPE is composed of plastically deformed microscopic crests, which are the main parts of the material that were submitted to wear. However, this estimation of the specific wear is in a very good agreement with the tendency achieved by the measurements of the material weight losses, carried out before and after tribological tests, although the measured values with this procedure were of the same order of magnitude of the statistical errors (~10^{-4} g).

2.5 Contact angles

The contact angles of the samples were measured using ultra-pure water and an automated contact angle measurement apparatus (OCA 15 Plus; Dataphysics, Germany).

3. Results and discussion

The thickness of the films was maintained between 1.1 and 2.3 μm. Table 1 shows the deposition conditions, chemical composition and some measured properties of the coatings. The composition analysis revealed a successful introduction of carbon and nitrogen in the coatings with the change of fluxes, as well as a wide range of silver content varying from 0 to 20 at. %. Table 1 also reports the ratio between the sum of carbon and nitrogen, and zirconium ((C+N)/Zr), allowing to group the samples depending on the amount of C+N excess with respect to a hypothetical stoichiometric ZrC_xN_{1-x} in the coatings. The first group consists of three samples deposited with the same acetylene and nitrogen fluxes varying only the Ag current density on the target (ZrCN1, ZrCN2 and ZrCN3). These samples have almost no excess of carbon and nitrogen (i.e. (C+N)/Zr ≈ 1). The second group formed by samples ZrCN4, ZrCN5 and ZrCN6 possesses an increasing carbon and nitrogen excess, allowing the presence of amorphous C-C and/or C-N phases in the coatings. The set of samples will be referred hereafter as ZrCN/Ag or ZrCN/Ag/a-(C,N) for coatings with and without amorphous carbon-based phases,

respectively. With these two groups it will be possible to better understand the influence of the silver and amorphous carbon phases on the ZrC_xN_{1-X} mechanical and tribological properties.

3.1 Structural and morphological characterization

The evaluation of the coating structure by X-ray diffraction and Raman spectroscopy revealed a mixture of crystalline and amorphous phases. Figs. 1a and 1b show the evolution of the crystalline phases and the Raman shift as a function of the (C+N)/Zr ratio of the samples. XRD diffraction pattern is in agreement with the presence of a face-centered cubic (FCC) ZrC_xN_{1-x} phase. The degree of crystallinity of the ZrC_xN_{1-x} phase is strongly dependent on the gas fluxes and the silver current density, showing lower grain sizes as silver and amorphous carbon phases are increased. In the bottom part of the graph, the ZrCN/Ag samples reveal a polycrystalline orientation and broadening of the ZrC_xN_{1-x} (200) peak due to the superposition of the diffraction plane (111) corresponding to an FCC Ag structure, clearly evidenced in sample ZrCN3 with 20 at. % of silver. This effect has been described in several works [33-35] and attributed to the immiscibility of silver with the ZrC_xN_{1-x} phase, segregating to the grain boundaries and hindering the crystal growth [36]. On the other hand, for ZrCN/Ag/a-(C,N) samples, the ZrC_xN_{1-x} crystalline phase exhibits a reduction of the grain sizes, as the (C+N)/Zr rises, down to a level that the carbonitride phase practically disappears (ZrCN6). Most probably this phase will have a very low grain size (lower than 1-2 nm) and, hence, undetectable by XRD.

Fig. 1b shows the Raman spectra of the deposited films in the range of 200-2000 cm^{-1}. The presence of disordered carbon-based phases is manifested by two signals located close to 1335 cm^{-1} and 1570 cm^{-1}, corresponding to the D (disordered) and G (graphitic) bands of disordered carbon, respectively [37]. The intensity of the Raman band at 1570 cm^{-1} was found to exhibit a

linear correlation with the (C+N)/Zr ratio measured by EPMA, indicating that a rough calculation of phase percentages could be carried out through the EPMA composition, described in the experimental section. The repartition of the atoms into the different possible phases is plotted in Fig. 2. This graph is useful to have a global overview of the phase composition necessary to establish correlations with the coating functional properties.

Fig. 3 depicts the SEM images in cross-section and surface views of the coatings. The cross-section images of the coatings show mostly a columnar growth with less defined columns as silver and a-(C,N) phases increase. For ZrCN/Ag samples with higher content of silver, the very small bright spots are believed to be silver nanoparticles. These white areas are also evident in the ZrCN/Ag/a-C coatings both in surface and cross-section images.

The surface morphology is much more compact as the amorphous phases rise in the samples ZrCN/Ag/a-(C,N), revealing a predominant effect of amorphous phases in controlling the morphology of the coatings as compared with silver. This effect can be explained by the ability of carbon phases to surround the ZrC_xN_{1-x} crystal in a composite-like configuration, in contrast to the silver phase, which tends to segregate and coalesce as isolated nanoparticles.

Previous publications have highlighted the ability of silver to segregate to the surface in similar matrices, particularly with the increment of the silver content [38] and time (aging) [39]. However, the Ag-ZrC_xN_{1-x} samples prepared in this work did not reveal a similar phenomenon, since none of the samples has shown the presence of silver aggregates on the surface. This fact should be taken into account when comparing the tribological behavior with reported data as the self-lubricating properties of such soft metallic phase cannot be regarded.

3.2 Mechanical and tribological characterization

3.2.1 Hardness

The hardness properties are correlated with the structural and morphological characteristics of the films. This property has been reported to depend on the ratio between the soft and hard phases in the coatings [40]. As described in the structural characterization, the films are mainly composed of three phases, metallic Ag, a-(C,N) and ZrC_xN_{1-x}. The plot of film hardness vs. ZrC_xN_{1-x} phase percentage gives a linear correlation (cf. Fig. 4). This hardness reduction with the diminution of the ZrC_xN_{1-x} phase percentage in the film, points out the ratio between hard and soft phases as the key-feature controlling the hardness properties, independently of the relative proportion between the silver and amorphous carbon phases. Previous works have already highlighted the negative influence of both silver and carbon amorphous phases on the hardness properties [33, 34, 40, 41]. However, in order to discriminate the influence of silver and amorphous carbon on the hardness separately, a multiple linear regression was carried out using the Ag and a-(C,N) contents. These calculations found a linear regression with a confidence level greater than 95% ($p<0.05$) and $R^2=0.994$ (cf. equation 1).

$$H = 20.35 - 0.385\, Ag\ phase - 0.204\, a-(C,N)\ phase\ [GPa] \quad (1)$$

This empiric mathematical correlation (Eq. 1) revealed that the effect of silver on hardness reduction is almost twice the carbon phase. It must be stressed that this correlation is only valid for the silver and a-(C, N) percentage ranges studied in this work.

3.2.2 Coefficient of friction

Fig. 5 plots the dependence of the average COF measured for each sample versus the content of a-(C,N) phase, Rq roughness and hardness. In both cases, the lowest value is obtained with the uncoated substrates pointing the importance of the surface properties in determining the mechanical strength of a material. Among the Ag-ZrC_xN_{1-x} samples, a significant reduction in

the COF is observed when a-(C,N) is present. This diminution could be explained in a boundary lubrication regime (that can be expected in these lubricated tests), since the presence of this phase between surface asperities in close contact, where the liquid media could not get access or be hindered, would lead to a decrease in the friction. It is well known the low friction values achieved with C-based coatings in dry sliding; however, a reduction of friction is also observed from 0.15 to 0.12 in the absence of the a-(C,N) phase, implicating that this should not be the only factor influencing the values of the COF. Fig. 5b and c depicts the tendencies of COFs with the film roughness and hardness values, respectively. The observed increase of the measured COFs with these properties can be understood as a dominant ploughing component affecting the friction forces. Hard and rough surfaces create more interlocking points than soft smooth surfaces, and thus when rubbing the films material again a softer polymer, as the UHMWPE used in the prostheses, a severe plastic deformation occurs and ploughs out a groove. This action creates a resistance to motion and therefore, the higher the hardness and the roughness, the higher the measured friction value is.

In addition to the material properties, the composition of the fluid is known to play an important role in the measurement of the COF of the tribological system due to chemical and/or physical interaction with the material surface. Albumin has demonstrated to protect the surface of the materials against wear; however, its role on the COF is not well understood. Fang et al. [22], for instance, have reported that the absorption of albumin on both UHMWPE and CrCoMo surfaces may induce an increase of the COF due to the interaction between the molecules of albumin. Contrarily, Hall et al. [18] and others [19, 20] have reported that the protection of albumin reduced both wear and COF. Despite of being a very complex process that depends on fluid pH, ionic strength and temperature [19], as well as on the hydrophobicity of the surface, several

reports agree that the albumin adsorbs easier to hydrophobic surfaces than hydrophilic materials [19, 23]. In this case, the contact angle of each film, and the stainless steel, were evaluated in order to investigate the correlation between the adsorption of the albumin with the hydrophobic behavior of the coatings. The results showed that the only hydrophilic surface (ZrCN1) has the highest COF. However, among the other samples with similar hydrophobicity levels (see Table 1); the COFs did not show a clear correlation with the contact angle. This certainly means that the effect of ploughing in friction should be given more consideration than the decrease of adhesion forces by effect of chemical bonded layers (albumin) or solid lubricant (amorphous carbon-based phases).

3.2.3 Wear

The wear of the UHMWPE counterpart was evaluated by measuring the permanent scar left at the end of the tribological test.

The UHMWPE wear rate did not exhibit significant differences between the samples (1.4 to 2.0 $x10^{-6}$ mm^3 N^{-1} m^{-1}), hampering the analysis of the surface roughness, hardness and COF effects on the polymer wear, probably explained due to the formation of a protective albumin layer adsorbed on the material surfaces. Nonetheless, the UHMWPE wear rate shows a particular trend as a function of the silver content, indicating that the wear of the UHMWPE increases by increasing the silver content in the films, as seen in Fig. 6. Recent investigations have found that silver nanoparticles on surfaces may delay the adsorption of the albumin [42], and therefore, the system may be less protected by the albumin as the silver nanoparticles increase in the material. The hydrophobic character of the samples also influences the albumin adsorption, as explained in previous section, thus, the high wear rate exhibited by the sample ZrCN1 may also be due to low

albumin adsorption as it is indeed the single sample showing a hydrophilic character. In summary, the wear of the soft UHMWPE material results from the balance between abrasive wear and plastic deformation, as determined by the film hardness, microasperities and debris particles, and boundary lubrication by albumin, controlled by the silver content and hydrophilic/hydrophobic character.

The wear rate of the films was not measurable in the present conditions, and therefore, the effect of phase composition (ZrC_xN_{1-x}, Ag and a-(C, N) phases) on the film wear could not be concluded.

SEM examination of the film wear tracks and UHMWPE ball scars of two representative samples (ZrCN1 and ZrCN4), belonging to the ZrCN/Ag and ZrCN/Ag/a-(C,N) groups respectively, are shown in Fig. 7. Although it is frequently reported the transfer of UHMWPE material to the counterpart, none of the samples showed the presence of transferred polymer material, as shown in Fig. 7, fact explained by in the wiping effect of the lubricant [18].

The wear debris are usually reported in the ranges of 0.1 to 100 μm [43], still being controversial the ability of the submicrometer particles to generate inflammatory response that results in osteolysis [44]. In this study the wear debris from the polymer or films could not be detected either in the fluid or on the surface of the materials, analyzed by STEM and SEM imaging, respectively. Thus, it is believed that the size of the particles is below 100 nm, since the roughness of the films were below 100 nm, and hence, the abrasive crests of the films only trim nanometric parts of the polymer.

Raman spectroscopy performed in both the film wear track and the rubbed UHMWPE did not show any significant changes after the tribological test, as shown in Fig. 8. However, the

UHMWPE exhibits an increasing oxygen content trend as the wear rate increases as shown in Fig. 9, which may be related to the polymer degradation, since the mechanical solicitation may promote the formation of radicals through bond scission, inducing the UHMWPE oxidation [45].

4. Conclusions

Ag-ZrC_xN_{1-x} coatings were produced by DC reactive magnetron sputtering, varying the silver content between 0 and 20 at. %. The coatings exhibited crystalline ZrC_xN_{1-x} phase, crystalline silver nanoparticles and amorphous carbon phases, being the latter two responsible for a reduction of the ZrC_xN_{1-x} grain sizes, an improvement of the films density and a reduction of the hardness, with their increment. Nonetheless, the amorphous carbon phases revealed a larger effect controlling both features, as compared to silver.

The COFs revealed a dominant ploughing mechanism on the friction forces dependent on the roughness and hardness of the films. No wear rate was measurable on the coatings and the UHMWPE wear rate did not exhibit significant differences between the samples, attributed to the formation of a protective layer of albumin on the material surface. The small variance of the UHMWPE wear rate was correlated to this protective layer, which is dependent on the hydrophobic/hydrophilic surface character as well as on the silver content.

The results support the idea of utilizing Ag-ZrC_xN_{1-x} coatings as a surface modification option for multifunctional purposes, adding functions such antimicrobial effect, corrosion resistance and maintaining or even improving their mechanical and tribological performance.

Acknowledgements

This research is partially sponsored by FEDER funds through the program COMPETE-Programa Operacional Factores de Competitividade and by Portuguese national funds through FCT-Fundação para a Ciência e a Tecnologia, under the projects ANTIMICROBCOAT - PTDC/CTM/102853/2008 and in the framework of the Strategic Projects PEST-C/FIS/UI607/2011", PEST-C/EME/UI0285/2011 and SFRH/BD/80947/2011. This work has also been supported by the Spanish MEC through the Consolider FUNCOAT (CSD2008-00023) project and Junta de Andalucía (P10-TEP-67182 project).

References

[1] R. Hauert, K. Thorwarth, G. Thorwarth, Surface and Coatings Technology, 233 (2013) 119-130.
[2] B. Subramanian, C.V. Muraleedharan, R. Ananthakumar, M. Jayachandran, Surface and Coatings Technology, 205 (2011) 5014-5020.
[3] W. Shi, H. Dong, T. Bell, Materials Science and Engineering: A, 291 (2000) 27-36.
[4] A. Betts, D. Dowling, M. McConnell, C. Pope, Materials & design, 26 (2005) 217-222.
[5] A.M. El-Kady, A.F. Ali, R.A. Rizk, M.M. Ahmed, Ceramics International, 38 (2011) 177-188.
[6] C.N. Lok, C.M. Ho, R. Chen, Q.Y. He, W.Y. Yu, H. Sun, P.K.H. Tam, J.F. Chiu, C.M. Che, Journal of Biological Inorganic Chemistry, 12 (2007) 527-534.
[7] P. Kelly, H. Li, P. Benson, K. Whitehead, J. Verran, R. Arnell, I. Iordanova, Surface and Coatings Technology, 205 (2010) 1606-1610.
[8] H. Cao, X. Liu, F. Meng, P.K. Chu, Biomaterials, 32 (2011) 693-705.
[9] D. Dowling, A. Betts, C. Pope, M. McConnell, R. Eloy, M. Arnaud, Surface and Coatings Technology, 163 (2003) 637-640.
[10] G.-N. Dong, M. Hua, J. Li, K.B. Chuah, Materials & Design, 28 (2007) 2402-2416.
[11] M.E. Turell, G.E. Friedlaender, A. Wang, T.S. Thornhill, A. Bellare, Wear, 259 (2005) 984-991.
[12] T. Goswami, S. Alhassan, Materials & Design, 29 (2008) 289-296.
[13] A. Buford, T. Goswami, Materials & Design, 25 (2004) 385-393.
[14] W. Rostoker, J. Galante, Journal of biomedical materials research, 13 (1979) 957-964.
[15] D.-W. Kim, K.-Y. Lee, Y. Jun, S. Lee, C. Park, Int. J. Precis. Eng. Manuf., 12 (2011) 1111-1118.
[16] H.J. Cho, W.J. Wei, H.C. Kao, C.K. Cheng, Materials Chemistry and Physics, 88 (2004) 9-16.
[17] C. Myant, P. Cann, Journal of the Mechanical Behavior of Biomedical Materials, 34 (2014) 338-348.
[18] R.M. Hall, A. Unsworth, Biomaterials, 18 (1997) 1017-1026.
[19] M.P. Gispert, A.P. Serro, R. Colaço, B. Saramago, Wear, 260 (2006) 149-158.
[20] M.P. Gispert, A.P. Serro, R. Colaço, A.M.B. do Rego, E. Alves, R.C. da Silva, P. Brogueira, E. Pires, B. Saramago, Wear, 262 (2007) 1337-1345.
[21] C.F.A. Alves, F. Oliveira, I. Carvalho, A.P. Piedade, S. Carvalho, Materials Science and Engineering: C, 34 (2014) 22-28.
[22] H.-W. Fang, M.-C. Hsieh, H.-T. Huang, C.-Y. Tsai, M.-H. Chang, Colloids and Surfaces B: Biointerfaces, 68 (2009) 171-177.
[23] K. Wang, C. Zhou, Y. Hong, X. Zhang, Interface Focus, 2 (2012) 259-277.

[24] M. Balaceanu, T. Petreus, V. Braic, C.N. Zoita, A. Vladescu, C.E. Cotrutz, M. Braic, Surface and Coatings Technology, 204 (2010) 2046-2050.
[25] C.-S. Chen, C.-P. Liu, Journal of Non-Crystalline Solids, 351 (2005) 3725-3729.
[26] M. Braic, V. Braic, M. Balaceanu, C.N. Zoita, A. Kiss, A. Vladescu, A. Popescu, R. Ripeanu, Materials Chemistry and Physics, 126 (2011) 818-825.
[27] E. Grigore, C. Ruset, X. Li, H. Dong, Surface and Coatings Technology, 204 (2010) 1889-1892.
[28] F. Hollstein, D. Kitta, P. Louda, F. Pacal, J. Meinhardt, Surface and Coatings Technology, 142–144 (2001) 1063-1068.
[29] J.-D. Gu, P.-L. Chen, Surface and Coatings Technology, 200 (2006) 3341-3346.
[30] E. Silva, M. Rebelo de Figueiredo, R. Franz, R. Escobar Galindo, C. Palacio, A. Espinosa, S. Calderon V, C. Mitterer, S. Carvalho, Surface and Coatings Technology, 205 (2010) 2134-2141.
[31] M.M. Larijani, M.B. Zanjanbar, A. Majdabadi, Journal of alloys and compounds, 492 (2010) 735-738.
[32] S. Calderon V, R.E. Galindo, N. Benito, C. Palacio, A. Cavaleiro, S. Carvalho, Journal of Physics D: Applied Physics, 46 (2013) 325303.
[33] J.G. Han, H.S. Myung, H.M. Lee, L.R. Shaginyan, Surface and Coatings Technology, 174–175 (2003) 738-743.
[34] P. Basnyat, B. Luster, Z. Kertzman, S. Stadler, P. Kohli, S. Aouadi, J. Xu, S.R. Mishra, O.L. Eryilmaz, A. Erdemir, Surface and Coatings Technology, 202 (2007) 1011-1016.
[35] W. Gulbiński, T. Suszko, Surface and Coatings Technology, 201 (2006) 1469-1476.
[36] J. Musil, Surface and Coatings Technology, 125 (2000) 322-330.
[37] M. Braic, V. Braic, M. Balaceanu, A. Vladescu, C. Zoita, I. Titorencu, V. Jinga, Surface and Coatings Technology, 206 (2011) 604-609.
[38] R. Escobar Galindo, N.K. Manninen, C. Palacio, S. Carvalho, Anal Bioanal Chem, 405 (2013) 6259-6269.
[39] N.K. Manninen, F. Ribeiro, A. Escudeiro, T. Polcar, S. Carvalho, A. Cavaleiro, Surface and Coatings Technology, 232 (2013) 440-446.
[40] S.H. Yao, Y.L. Su, W.H. Kao, K.W. Cheng, Surface and Coatings Technology, 201 (2006) 2520-2526.
[41] J.C. Sánchez-López, M.D. Abad, I. Carvalho, R. Escobar Galindo, N. Benito, S. Ribeiro, M. Henriques, A. Cavaleiro, S. Carvalho, Surface and Coatings Technology, 206 (2012) 2192-2198.
[42] P. Kumari, P. Majewski, Journal of Nanomaterials, 2013 (2013).
[43] S. Ge, S. Wang, N. Gitis, M. Vinogradov, J. Xiao, Wear, 264 (2008) 571-578.
[44] A.E.a.A.S.S. Hamid Reza Seyyed Hosseinzadeh, The Bearing Surfaces in Total Hip Arthroplasty – Options, Material Characteristics and Selection, in: D.S. Fokter (Ed.) Recent Advances in Arthroplasty, INTECH, 2012.
[45] S.M. Kurtz, The UHMWPE handbook: ultra-high molecular weight polyethylene in total joint replacement, Access Online via Elsevier, 2004.

Figure Captions

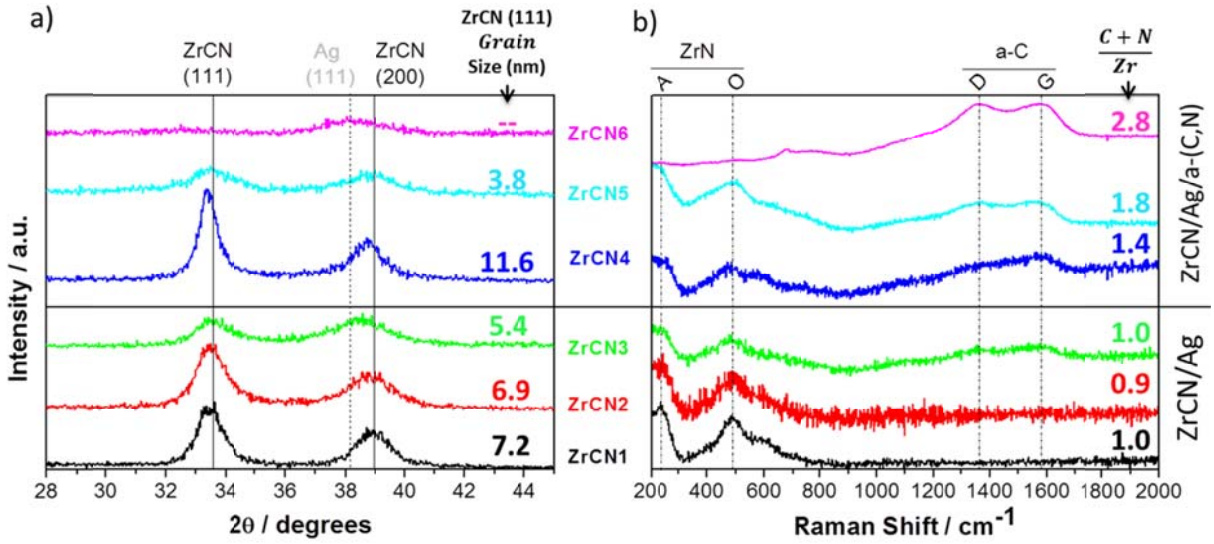

Fig. 1 a) Coatings X-ray diffractograms, ZrC0.5N0.5 diffraction pattern (ICDD-03-065-8779) and Ag diffraction pattern (ICDD- 00-087-0719) are shown for comparison and b) coatings Raman spectroscopy as a function of the (C+N)/Zr ratio.

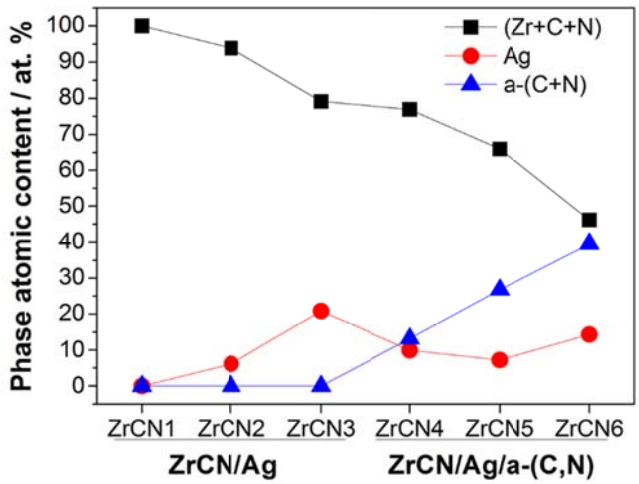

Fig. 2 Phase atomic composition calculated by EPMA. (Zr+ C+ N), a-(C+N) and Ag atomic percentages are associated to the ZrCxN1-x, amorphous carbon and silver phases, respectively.

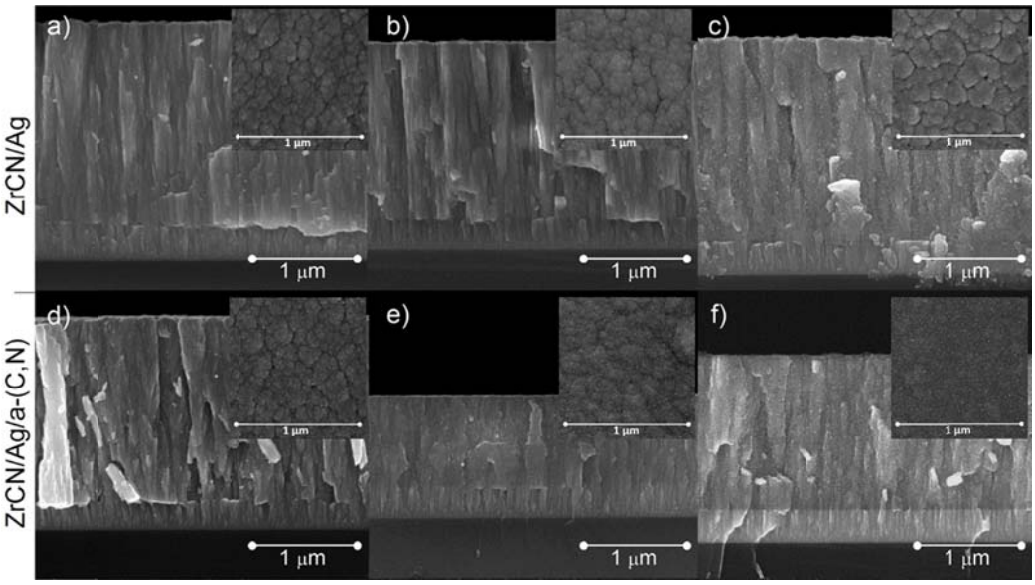

Fig. 3 Surface and cross-section SEM images for Ag-ZrC_xN_{1-x} coatings a) ZrCN1, b) ZrCN2, c) ZrCN3, d) ZrCN4, e) ZrCN5 and f) ZrCN6

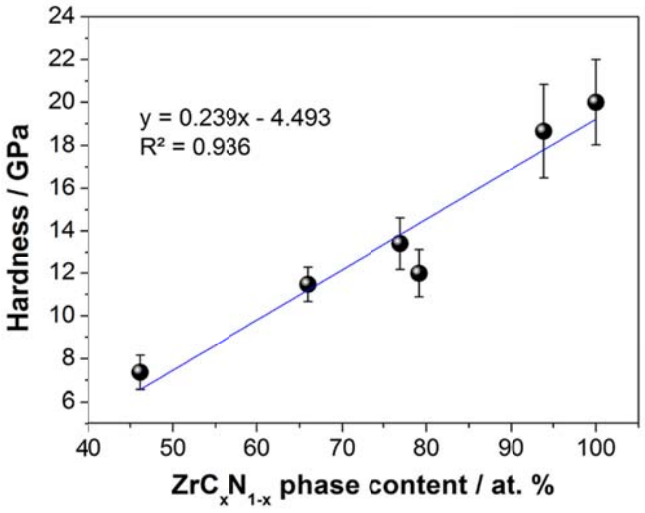

Fig. 4 Films hardness evolution as a function of ZrCxN1-x phase content with its correspondent linear regression

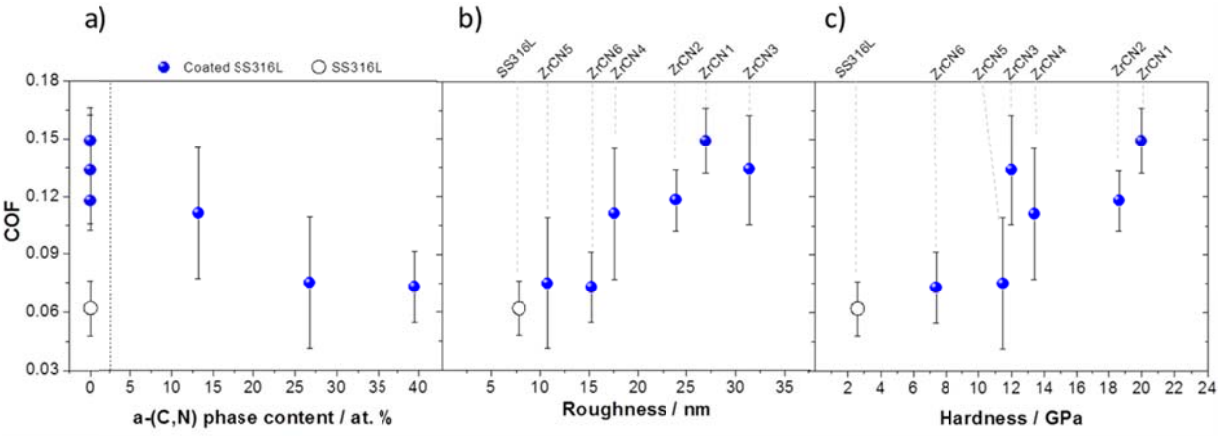

Fig. 5 a) Films-UHMWPE coefficient of friction evolution as a function of a) carbon amorphous phases content , b) roughness and c) hardness of the coatings.

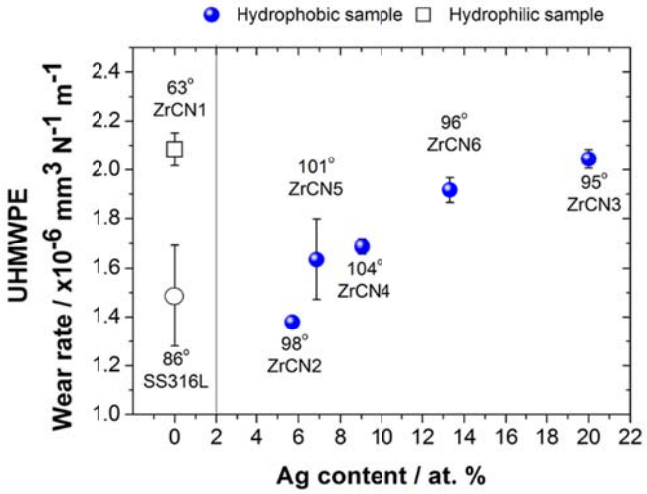

Fig. 6 Films-UHMWPE wear factor evolution as a function of the silver content. The values in degrees represent the contact angle of each sample.

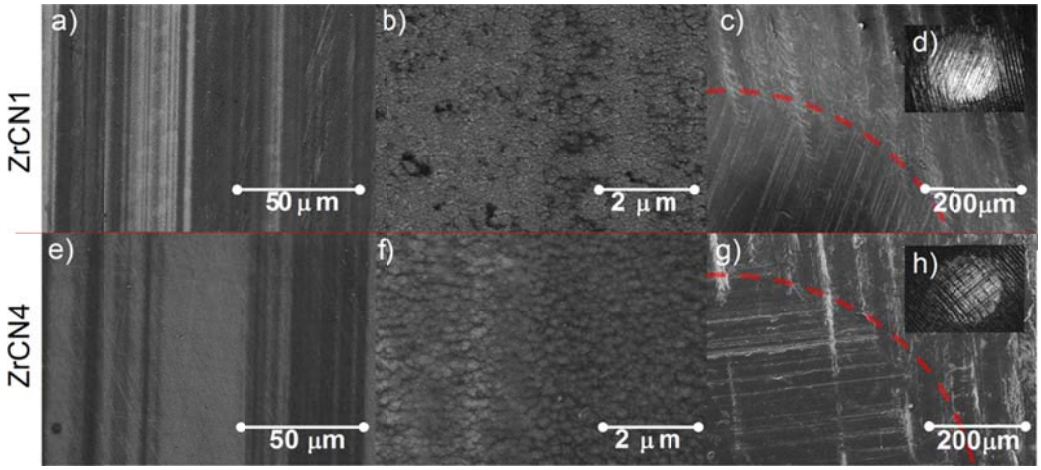

Fig. 7 Scanning electron microscope images of the wear track on the films and wear mark on the UHMWPE of two representative samples a) and b) wear track of ZrCN1, c) wear mark on the UHMWPE used against sample ZrCN1, d) and e) wear track of ZrCN4, f) wear mark on the UHMWPE used against sample ZrCN4. Optical images of the UHMWPE scar rubbed against g) ZrCN1 and h) ZrCN4.

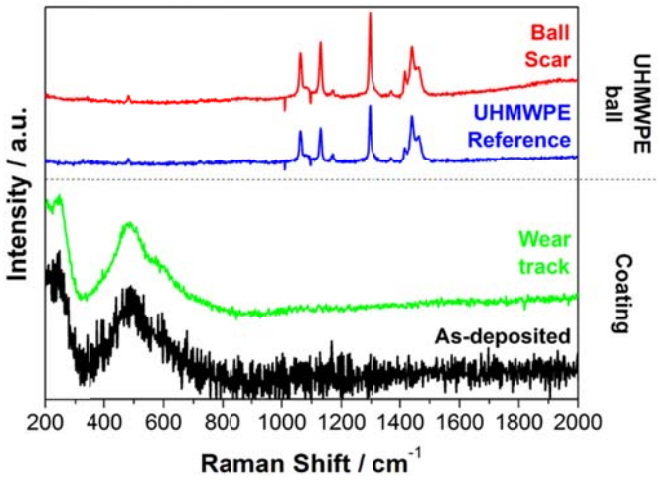

Fig. 8 Raman spectroscopy before and after the tribological test for a representative sample (ZrCN2) and its corresponding UHMWPE counterpart.

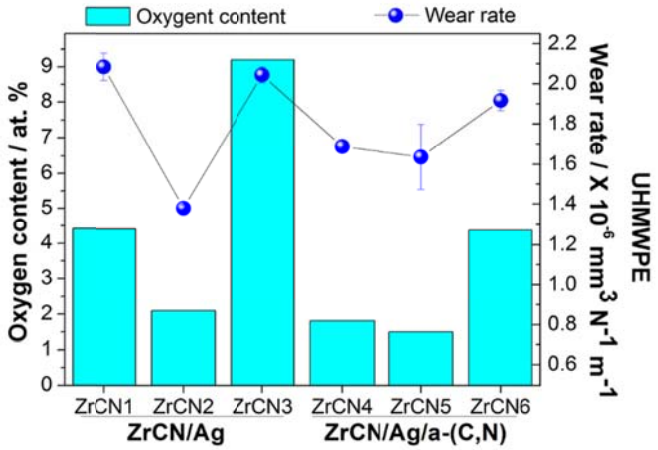

Fig. 9 Energy dispersive X-ray analysis of oxygen on the polymer wear mark.